Title

Heterogeneity of Network Structures and Water Dynamics in κ-Carrageenan Gels Probed by Nanoparticle Diffusometry.

Journal

Langmuir, 34(37)

Authors

de Kort, Daan

Schuster, Erich

Hoeben, Freek

et al.

Publication Date

2018-09-18

DOI

10.1021/acs.langmuir.8b01052

Peer reviewed

LANGMUIR Article
Cite This: Langmuir 2018, 34, 11110−11120
pubs.acs.org/Langmuir

Heterogeneity of Network Structures and Water Dynamics in κ-Carrageenan Gels Probed by Nanoparticle Diffusometry

Daan W. de Kort,[†,‡] Erich Schuster,[§,∥] Freek J.M. Hoeben,[‡,⊥] Ryan Barnes,[#] Meike Emondts,[#] Henk M. Janssen,[‡,⊥] Niklas Lorén,[§,∥,¶] Songi Han,[#] Henk Van As,[†,‡] and John P.M. van Duynhoven[*,†,‡,▽]

[†]Laboratory of Biophysics, Wageningen University, Stippeneng 4, 6708 WE Wageningen, The Netherlands
[‡]TI-COAST, Science Park 904, 1098 XH Amsterdam, The Netherlands
[§]Product Design and Perception, RISE Agrifood and Bioscience, Box 5401, S-402 29 Göteborg, Sweden
[∥]SuMo Biomaterials, VINN Excellence Centre, and [¶]Department of Physics, Chalmers University of Technology, SE-412 96 Göteborg, Sweden
[⊥]SyMO-Chem B.V., Het Kraneveld 4, 5612 AZ Eindhoven, The Netherlands
[#]Department of Chemistry and Biochemistry, University of California, Santa Barbara, Santa Barbara, California 93106, United States
[▽]Unilever R&D, Olivier van Noortlaan 120, 3133 AT Vlaardingen, The Netherlands

Supporting Information

ABSTRACT: A set of functionalized nanoparticles (PEGylated dendrimers, d = 2.8−11 nm) was used to probe the structural heterogeneity in Na^+/K^+ induced κ-carrageenan gels. The self-diffusion behavior of these nanoparticles as observed by ^1H pulsed-field gradient NMR, fluorescence recovery after photobleaching, and raster image correlation spectroscopy revealed a fast and a slow component, pointing toward microstructural heterogeneity in the gel network. The self-diffusion behavior of the faster nanoparticles could be modeled with obstruction by a coarse network (average mesh size <100 nm), while the slower-diffusing nanoparticles are trapped in a dense network (lower mesh size limit of 4.6 nm). Overhauser dynamic nuclear polarization-enhanced NMR relaxometry revealed a reduced local solvent water diffusivity near 2,2,6,6-tetramethylpiperidin-1-oxyl (TEMPO)-labeled nanoparticles trapped in the dense network, showing that heterogeneity in the physical network is also reflected in heterogeneous self-diffusivity of water. The observed heterogeneity in mesh sizes and in water self-diffusivity is of interest for understanding and modeling of transport through and release of solutes from heterogeneous biopolymer gels.

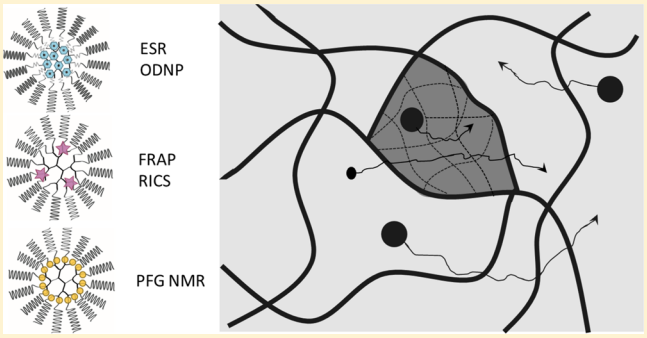

INTRODUCTION

Biopolymer hydrogels constitute cross-linked, percolating networks, giving rise to a porous and tortuous microstructure. Structural descriptors of these microstructures can be obtained from the reduced self-diffusivity of nonsticky nanoparticles with diameters on the order of the network mesh size.[1,2] These descriptors of the microstructure complement spatial insights obtained by optical or electron microscopy.[1] If the nanoparticles are larger than the structural features of the polymer network, they are immobilized.[1,3,4] If the size of the nanoparticles is smaller than, but on the order of the distance between the polymer strands or fibers, the nanoparticles are still free to diffuse in the water phase, but their mobility will be determined by obstruction imposed by the polymer strands, as well as by the local solvent properties. Several physical models have been introduced to relate the reduced self-diffusion coefficients of nanoparticles in hydrogels to the polymer concentration (volume fraction), polymer strand thickness, nanoparticle diameter, and network mesh size.[5−7] "Obstruction effect"-type models imply that the rigid polymer network is tortuous and imposes an increased path length for nanoparticles moving between two points in the network but do not account for interactions between the nanoparticles and the polymer strain.[1] Other models provide scaling laws for the hydrodynamic friction of the nanoparticles and the polymer chains owing to nonnegligible attractive interactions.[1] All these models predict the convergence to a long-term, average diffusion coefficient (assuming simple Brownian motion). To date, however, none of these models have considered the effects of network heterogeneity, in particular, at the nm length

Received: March 31, 2018
Revised: August 15, 2018
Published: August 22, 2018

DOI: 10.1021/acs.langmuir.8b01052
Langmuir 2018, 34, 11110−11120

scale, and none have considered the existence of spatially heterogeneous solvent water self-diffusivity within the heterogeneous network.

In this work, we explore the use of nanoparticle diffusometry for the assessment of network heterogeneity in κ-carrageenan gels. κ-Carrageenan is a linear polysaccharide that is widely used industrially as a gelling agent. Gelation of κ-carrageenan occurs upon cooling a warm aqueous solution, during which the polymer coils first form helices that subsequently aggregate in a side-by-side manner.[8,9] The coil-to-helix transition, which is essential for eventual gelation, is very sensitive to binding of cations such as potassium, calcium, or sodium ions, which hence strongly influence the network heterogeneity of the gels and their elastic strength.[10] Electron microscopy has shown that the so-formed κ-carrageenan gel network[4,11] is heterogeneous, with co-existing coarser and denser networks.[8,10] Populations of slow and fast diffusing nonsticky nanoparticles[12,13] in these gels have been attributed to the heterogeneity of the gel strand network.[14] A pictorial representation consistent with this view, as well as with the current study, is given in Figure 1 for clarity—we will further discuss the veracity of this schematic on the basis of experimental results. In this work, we aim to quantify the physical as well as the solvent heterogeneity of the κ-carrageenan gel network at multiple length scales spanning the sub-nanometer to micrometer scale by using spectroscopically active, nonsticky nanoparticles (2.8−11 nm in diameter) as diffusional probes. In previous work, we have described the design of these nanoparticles and have validated that they are monodisperse and non-interacting with the κ-carrageenan gel matrix.[11] To study the bimodal diffusion of the nanoparticles, we use NMR diffusometry, fluorescence recovery after photobleaching (FRAP), and raster image correlation spectroscopy (RICS). NMR diffusometry provides a means to noninvasively obtain a bulk-averaged self-diffusion coefficient. FRAP and RICS allow spatially resolved mapping of self-diffusion coefficients; these techniques are complementary in the sense that they cover the large and small self-diffusion regimes, respectively. To assess solvent (water) diffusivity within this heterogeneous gel network, we deployed nanoparticles similar to the ones used in the other studies, except that they were now functionalized with paramagnetic 2,2,6,6-tetramethylpiperidin-1-oxyl (TEMPO) moieties. The presence of the paramagnetic TEMPO labels allows probing of water dynamics within two to three solvent layers (0.5−1 nm) from the surface of the nanoparticles by Overhauser dynamic nuclear polarization (ODNP)-enhanced NMR relaxometry.[15,16] Using this toolkit, we describe whether a physical, a solvent, or a combined model is needed to understand the apparent heterogeneity in the nanoparticle diffusivity within κ-carrageenan gel networks.

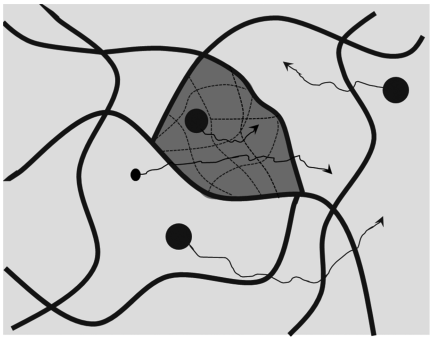

Figure 1. Schematic representation of self-diffusion of nanoparticles in coarse (10^2 nm mesh) and dense (>4.6 nm mesh) regions in κ-carrageenan gels. Larger nanoparticles can be immobilized in the dense regions (dark) but can also diffuse through the coarse network. Smaller nanoparticles can probe both the coarse and dense networks. Within the dense region (dark), self-diffusion of water is reduced.

MATERIALS AND METHODS

Sample Preparation. κ-Carrageenan gels were prepared by suspending κ-carrageenan powder (2 wt %) in a solution of sodium chloride (between 0 and 200 mM), potassium chloride (20 mM), and dendritic nanoparticles in water followed by stirring and heating to 80 °C for 15 min. The nanoparticles were dosed at 0.1−0.2 wt % for G1-^{19}F, G3-^{19}F, G5-^{19}F, 0.05 wt % for G5-ATTO 488, and 0.1 wt % of G5-TEMPO. The solutions were subsequently allowed to cool down to room temperature during which gelation (together with the nanoparticles) took place. "Washed" gels were prepared by keeping a ∼3 × 3 × 3 mm gel cube in a ∼50× larger volume of corresponding salt solution for a week and refreshing the medium daily. Washing had no apparent effects (swelling or shrinkage) on the gels.

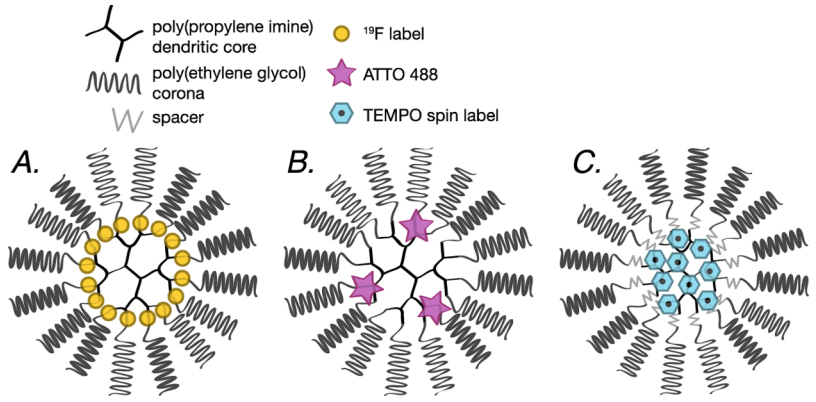

Figure 2. Schematic illustrations of nanoparticles with G5 PPI dendrimer cores used in this study (these illustrations are not intended to reflect the conformation of the nanoparticles in solution): (A) ^{19}F-labeled PEGylated dendrimers (G5-^{19}F, d = 6.9 nm) that can be observed by ^{19}F and ^{1}H NMR via the signal of the PEG corona, (B) PEGylated ATTO 488-labeled dendrimers (G5-ATTO 488, d = 6.0 nm, Supporting Information, section S2.4.1) that can be observed by FRAP and RICS, and (C) PEGylated TEMPO-labeled dendrimers for ODNP-enhanced NMR spectroscopy, with a spacer to slightly increase their diameter (G5-TEMPO, $d \approx 11$ nm).

DOI: 10.1021/acs.langmuir.8b01052
Langmuir 2018, 34, 11110−11120

Labeled Dendritic Nanoparticles. Besides ^{19}F-labeled PEGylated generation-1, -3, and -5 (G1-^{19}F, G3-^{19}F, and G5-^{19}F) poly(propylene imine) dendritic nanoparticles (d = 2.8, 4.6, and 6.9 nm, respectively) as presented and characterized in our previous work,[11] we prepared additional labeled analogs (SyMO-Chem B.V., Eindhoven, Netherlands). These nanoparticles contained a core based on a G5 dendrimer and a brush-like polyethylene glycol (PEG) corona, where the labels were introduced underneath the PEG corona. One particle contained ATTO 488 fluorescent dyes at the interface between the core and corona, while the other contained TEMPO spin labels and a spacer between the same core and corona, where a spacer was introduced to slightly increase the particle size. The diameter increase was aimed at increasing the fraction of immobilized nanoparticles in the κ-carrageenan gel (see the Results and Discussion section). The synthetic procedures are included in the Supporting Information, section S2, and cartoons of the three nanoparticles are presented in Figure 2, where the locations of the ^{19}F, ATTO 488, and TEMPO labels within the nanoparticles have been indicated.

Pulsed-Field Gradient NMR Diffusometry. Because of the high ^{1}H loading of the nanoparticles, spin echo pulsed-field gradient (SE-PFG) NMR measurements on ^{19}F-labeled dendrimers (G1-, G3-, and G5-^{19}F) were initially carried out on ^{1}H instead of ^{19}F. We used ^{1}H NMR because the ^{1}H NMR signal of the PEG corona provides a high signal intensity, while the signal of the rigid κ-carrageenan matrix can be filtered out because its associated T_2 is much shorter than that of the highly mobile PEG−^{1}H. ^{19}F NMR measurements, which have lower sensitivity and hence slightly longer acquisition times, were subsequently used to cross-check for the absence of the background signal in the ^{1}H NMR measurements. ^{1}H SE-PFG NMR and ^{19}F STE-PFG NMR experiments were performed with a Bruker Avance II spectrometer operating at 7 T B_0 magnetic field strength (resonance frequencies 300 MHz for ^{1}H and 282 MHz for ^{19}F), equipped with a Bruker Diff25 gradient probe [maximum PFG intensity 9.60 T/m]. The probe was equipped with a 10 mm RF insert tuned to the ^{1}H or ^{19}F resonance frequency. Experiments and data analysis were performed using standard procedures.[3] In short, ^{1}H SE-PFG NMR experiments were based on spin echo detection by stepwise variation of the gradient pulse amplitude at an effective gradient pulse duration of 5 ms, while keeping the diffusion-observation time between the gradient pulses at 200 ms. The minimum gradient amplitude was chosen to be high enough to attenuate the ^{1}H signal of water almost completely. The attenuation of the ^{1}H echo intensity of the PEG corona as a function of increasing gradient amplitude is described by a sum of Stejskal−Tanner-type exponentials $(I/I_0) = A\ e^{-bD}$ and $b = (\gamma\delta g)^2(\Delta - \delta/3)$, where (I/I_0) is the signal attenuation, D is the diffusion coefficient, γ is the gyromagnetic ratio, δ is the duration of the gradient pulse, g is the gradient amplitude, and Δ is the diffusion-observation time.[17] Error estimates of the self-diffusion coefficients D were obtained via bootstrap resampling as described previously.[11] Using the same experimental settings but starting from a lower initial gradient amplitude, so as not to suppress the water signal, ^{1}H SE-PFG NMR on water itself was performed in gels without dissolved nanoparticles. ^{19}F STE-PFG NMR experiments were based on stimulated echo detection with the same observation time but did not require suppression of the background signal.

According to the obstruction model of Johnson,[18] the κ-carrageenan polymer strand radius r_f can be obtained from the reduced diffusion coefficients D/D_0 using

$$\frac{D}{D_0} = \frac{e^{-0.84\alpha^{1.09}}}{1 + \left(\frac{r_s^2}{\kappa}\right)^{1/2} + \frac{1}{3}\frac{r_s^2}{\kappa}} \qquad \text{with } \alpha = \varphi\left(\frac{r_s + r_f}{r_f}\right)^2$$
$$\text{and } \kappa = 0.31 r_f^{\,2}\varphi^{-1.17} \tag{1}$$

where r_s is the nanoparticle radius and φ is the polymer volume fraction. A length scale for the mesh size d_m can be estimated from[19]

$$d_m = r_f\sqrt{\frac{3\pi}{\varphi}} \tag{2}$$

Fluorescence Recovery after Photobleaching. FRAP was carried out on the gels before washing. A Leica SP5 AOBS setup was used with a 10×, 0.4 NA water objective using the following settings: 1024 × 1024 pixels, a zoom factor of 6 (with a zoom-in during bleaching), and 1400 Hz, yielding a pixel size of 0.253 μm and an image acquisition rate of 0.372 s/image. The FRAP images were stored as 16 bit tif-images. A 488 nm Ar-laser was used to excite the ATTO 488-labeled dendritic nanoparticles. The bleached regions of interest (ROIs) were 50 μm large discs. The measurement routine consisted of 50 pre-bleach images, 10 bleaching images [wherein a high intensity laser pulse using all available laser lines (458, 476, 488, 496, 514, 561, and 633 nm) bleaches the fluorophores in the ROI], and 1000 post-bleach frames to record the fluorescence recovery. A FRAP model using a pixel-based likelihood framework[20] was utilized for data analysis.

Raster Image Correlation Spectroscopy. RICS[21] was carried out on washed gels only. A Leica SP5 AOBS setup was used with a 63×, 1.2 NA water objective using the following settings: 512 × 512 pixels, a zoom factor of 10, and a scan rate of 10 Hz, yielding a pixel size of 0.0482 μm and a pixel dwell time (t_P) of 0.48 ms. A 488 nm Ar-laser was used to excite the ATTO 488-labeled dendritic nanoparticles. The laser power on the stage was 10 μW during the experiments. The recorded RICS data were analyzed to yield one diffusion coefficient per 512 × 512 pixel data set. Furthermore, ca. 70 × 70 pixel-sized ROIs were analyzed separately in order to segment the data and estimate local diffusion coefficients.

Electron Paramagnetic Resonance and ODNP-Enhanced NMR Spectroscopy. cw-Electron paramagnetic resonance (EPR) spectra were measured on a Bruker EMX X-band spectrometer equipped with a cylindrical (TE011) cavity. Samples were irradiated at 9.8 GHz with the center field set at 3480 G and a sweep width of 150 G. The field modulation amplitude was kept below 0.2 times the center peak line width to acquire the intrinsic EPR lineshape and amplitude without distortion. Room-temperature N_2 gas was streamed through the cavity at 14 L/min for temperature control, and all spectra were acquired at 298 K.

Local water diffusion coefficients within 0.5−1 nm of nitroxide radical-based TEMPO spin labels were measured by ODNP-enhanced NMR relaxometry. The same samples and instrument were used as described for the X-band EPR experiments. The magnetic field and frequency for irradiation were set to the center resonance of the nitroxide EPR spectra. Samples were positioned in a home-built U-shaped NMR coil (Cu wire, 28 AWG) tuned to 14.8 MHz and connected to a broadband channel of a Bruker Avance NMR spectrometer, as described in detail elsewhere.[22,23] The longitudinal relaxation time of water−^{1}H, in the presence (T_1) and absence ($T_{1,0}$) of the nitroxide spin labels, was carefully measured using an inversion recovery pulse sequence. The ^{1}H NMR signal enhancement E of water was recorded as a function of increasing microwave power p that was varied using a home-built X-band microwave amplifier with a power output between 0.1 mW and 1.5 W. ^{1}H NMR spectra were integrated over their absorption peak and the absolute values plotted versus the input microwave power. We point the reader elsewhere[16,24] for a more comprehensive discussion and derivation of the manner in which the DNP data are processed to extract a local diffusion coefficient—here, we present a practical guide. The measured NMR signal enhancement $E(p)$ extrapolated to infinitely high microwave power ($E(\infty)$), together with T_1 and $T_{1,0}$, is used to extract the key DNP parameter termed the dipolar coupling factor (ξ), which corresponds to the dipolar electron−^{1}H cross relaxation efficiency with respect to all ^{1}H NMR relaxation processes. The manner in which the timescale of the local dynamics between the spin labels and the water protons affects the measured value of the dipolar coupling factor is contained in the spectral density function for the dipolar interaction between the spin label and the water protons—this function can be used to directly translate the coupling factor in a local correlation time τ_{dip} representing the translational diffusion dynamics

DOI: 10.1021/acs.langmuir.8b01052
Langmuir 2018, 34, 11110−11120

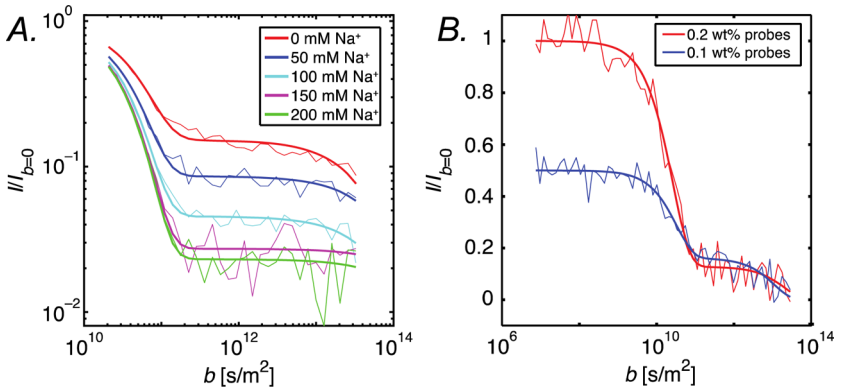

Figure 3. Plots of ^{1}H SE-PFG NMR signal attenuation ($I/I_{b=0}$) as a function of b for 0.1 wt % G5-^{19}F (d = 6.9 nm) nanoparticles in 2 wt % κ-carrageenan gels that were (A) induced at different Na^+ and constant 20 mM K^+ concentrations. The initial part of the curves is missing because a finite initial gradient amplitude was used to suppress the ^{1}H NMR signal of water and solutes with higher diffusion coefficients. The curves have been normalized to the back-predicted amplitude at zero gradient amplitude and fitted with a sum of two Stejskal−Tanner exponentials. Note that instead of a conventional Stejskal−Tanner plot, a double-logarithmic plot was used that turned out to provide a clearer view of the bimodal signal attenuation. (B) ^{19}F STE-PFG NMR signal decays of G5-^{19}F particles dosed at 0.1 and 0.2 wt % (blue and red curves, respectively) in 2 wt % κ-carrageenan gels induced with 0 mM Na^+ and 20 mM K^+ concentrations.

of the local water in the dipolar coupling vicinity of the spin label. The analytical expression for the dependency of coupling factor ξ on the spectral density function J is given by

$$\xi = \frac{6J(\omega_e - \omega_H; \tau_{dip}) - J(\omega_e + \omega_H; \tau_{dip})}{6J(\omega_e - \omega_H; \tau_{dip}) + 3J(\omega_H; \tau_{dip}) + J(\omega_e + \omega_H; \tau_{dip})} \quad (3)$$

wherein ω_e and ω_H are the electron and proton Larmor frequencies, respectively, and J is the spectral density function given by the force free hard sphere model[25]

$$J = \left(1 + \frac{5\sqrt{2}}{8}(\omega\tau)^{1/2} + \frac{\omega\tau}{4}\right)\left(1 + (2\omega\tau)^{1/2} + \omega\tau + \frac{\sqrt{2}}{3}(\omega\tau)^{3/2} + \frac{16}{81}(\omega\tau)^2 + \frac{4\sqrt{2}}{81}(\omega\tau)^{5/2} + \frac{(\omega\tau)^3}{81}\right)^{-1} \quad (4)$$

As demonstrated elsewhere,[24] coupling factor ξ can be separated into two relaxation rates k_σ and k_ρ

$$\xi = \frac{k_\sigma}{k_\rho} \quad (5)$$

The two relaxation rates can be accessed experimentally because they are related to measurable parameters via

$$k_\sigma = C^{-1}\frac{\omega_H}{\omega_e S_{max}}\frac{E(\infty)}{T_1} \quad (6)$$

$$k_\rho = C^{-1}(T_1^{-1} - T_{1,0}^{-1}) \quad (7)$$

where C is the concentration of the unpaired electron of the spin labels and S_{max} is the maximal electron spin saturation factor.

Local diffusion coefficients D were determined via the relation

$$D = \mu^2/\tau_{dip} \quad (8)$$

where μ = 3.0 Å represents the distance of the closest approach of the water to the radical electron spin label.[15,23] The experimental error on the DNP measurements is approximated to fall between 3 and 5% from the quality of the curves fitted to extract $E(\infty)$ and T_1.

RESULTS AND DISCUSSION

Network Heterogeneity Probed by Nanoparticle PFG NMR Diffusometry. In previous work, we have shown that the self-diffusion coefficients of nonsticky ^{19}F-labeled G1-, G3-, and G5-nanoparticles with diameters of 2.8−6.9 nm decrease with the increased κ-carrageenan concentration.[11,19] In the current work, we carried out NMR diffusometry experiments using the same nanoparticles in gels induced at lower sodium concentrations (≤200 mM Na^+)—it is well-established that this condition results in a more heterogeneous network structure.[13] For these experiments, performed with G1-, G3-, and G5-^{19}F nanoparticles (d = 6.9 nm), we used a single κ-carrageenan concentration of 2 wt %, a K^+ concentration of 20 mM, and a varied Na^+ concentration. The resulting ^{1}H SE-PFG NMR attenuation curves for G5-^{19}F nanoparticles are shown in Figure 3A. At 0, 50, and 100 mM Na^+ concentrations, a significant amplitude offset is seen at higher b-values, while this offset is hardly visible at 150 and 200 mM Na^+ concentrations. This indicates that at lower Na^+ concentrations, a significant fraction of G5-^{19}F particles become immobilized. In order to quantify this effect, a sum of two exponentials was fitted to describe the shape of the attenuation curves. In recent work,[11] we have shown that this is an adequate approach to quantify multimodal self-diffusive behavior of nanoparticles. The offset is not flat, but slightly decreases as a function of b, indicating that the slower G5-^{19}F nanoparticles are not completely stationary on the time scale of the experiment (200 ms). Furthermore, a biexponential fit seems to be not optimal for the 0 mM Na^+-curve, suggesting that the slower particle fraction component represents a distribution of low diffusion coefficients, and not complete immobilization ($D \approx 0$ m^2/s) of particles over the Δ = 200 ms diffusion-observation time. No slow-diffusing fraction was observed for the smaller G1-^{19}F (d = 3.4) and G3-^{19}F (d = 4.6 nm) nanoparticles with a similar nonsticky design as the G5-^{19}F nanoparticles (see the Supporting Information, section S4). This indicates that the immobilization of nanoparticles is size-dependent, which is known to occur when diameters of nanoparticles approach the mesh sizes in hydrogels.[2,26] In Figure 3B, ^{19}F STE-PFG NMR attenuation curves are shown for a gel induced with 0 mM Na^+ (and a base concentration of 20 mM K^+, as before) with G5-^{19}F nanoparticles, now at two different particle concentrations of 0.1 and 0.2 wt %. The results show that a 2-fold difference in the G5-^{19}F nanoparticle concentration has no effect on the amplitude of the slow

DOI: 10.1021/acs.langmuir.8b01052
Langmuir 2018, 34, 11110−11120

particle fraction, while the amplitude of the rapid fraction increases by a factor of 2. This indicates preferential partitioning of G5-^{19}F nanoparticles into the dense network of κ-carrageenan. In previous work, we established that the coating of the G1, G3, and G5-^{19}F particles with ethoxylate groups was effective in preventing attractive interactions with the κ-carrageenan matrix.[11] A common observation for nanoparticles diffusing in gels is that a fraction becomes immobilized, which was attributed to the presence of matching voids within heterogeneous networks.[2,26] Recent modeling work established that no strong interactions are needed to promote trapping of particles in matching voids in heterogenous gel networks,[27] which is in agreement with our current explanation of immobilization of a fraction of the G5 particles in heterogeneous κ-carrageenan networks. In this model, all available voids are occupied by the particles before the surplus can move freely through the coarser network. Because the ratio between the particle concentration and available voids in the dense network is difficult to control, care should be taken with directly deriving the phase volumes of dense and coarse networks from the fraction of slow nanoparticles.

The reduced diffusion coefficients (D/D_0) obtained from a two-component fit to the PFG decays shown in Figure 3A are summarized in Figure 4A. The plot shows that the slower fraction displays diffusion coefficients for the G5-^{19}F nanoparticles that are more than 3 orders of magnitude lower ($\sim 10^{-14}$ m^2/s) than the faster fraction ($\sim 10^{-11}$ m^2/s). These diffusion constants were measured using Δ = 200 ms for the diffusion-observation time window, which implies that for the faster diffusing nanoparticles, the root-mean-square-displacement (rmsd), $(2Dt)^{1/2}$, of the nanoparticles is >5 μm. From the reduced diffusion constants (D/D_0) of this faster diffusing G5-^{19}F nanoparticle fraction, the average mesh sizes of the coarse network can be estimated using Johnson's obstruction model.[18] These mesh sizes were on the order of tens-of-nm, and are presented in Figure 4B. These mesh sizes correspond to the coarse network schematically presented in Figure 1. The lower limit of the mesh size of the dense network can also be estimated from the diameter of the largest nanoparticle (G3) that does *not* get trapped, that is, 4.6 nm (indicated as a dashed line in Figure 4B). The rmsd of the slower fraction over the course of Δ = 200 ms lies in the tens-of-nm range, indicating that in this time window, the G5-^{19}F particle can move only several times its diameter (6.9 nm) in the dense network depicted in Figure 1 (dark gray domain). Such small displacements suggest pore hopping mechanisms[26] and/or small movements of the dense network itself,[28] so for the slow-diffusing fraction, we refrained from using Johnson's obstruction model to estimate a mesh size because it demands elastic collisions.

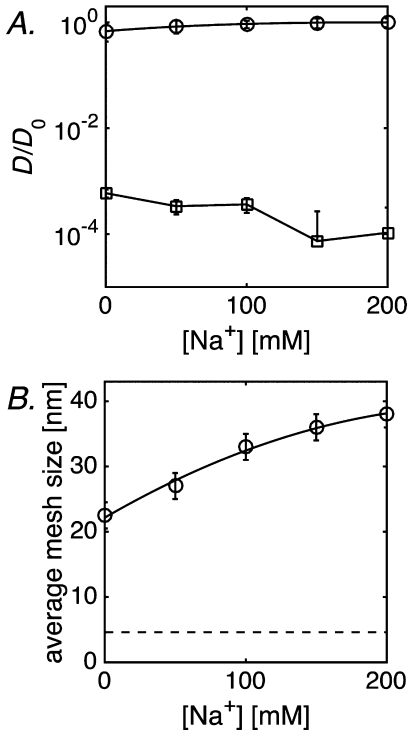

Figure 4. (A) Self-diffusion coefficients D of G5-^{19}F (d = 6.9 nm) nanoparticles (0.1 wt %) in 2 wt % κ-carrageenan gels induced at different Na^+ concentrations and a constant 20 mM K^+ concentration (normalized to the diffusion coefficient in water, 5×10^{-11} m^2/s); both the faster (○) and slower (□) fractions are indicated. (B) Mesh sizes for the coarse network (○) as estimated by Johnson's obstruction model; the lower limit of the mesh size of the dense network is indicated with a dashed line.

Next, we kept the κ-carrageenan gel cubes (approximately 3 × 3 × 3 mm) in a much larger volume of salt solution and waited for a week, while daily refreshing the salt medium, to allow all nontrapped nanoparticles to escape from the gel. Upon washing, the faster component could not be observed anymore in the PFG attenuation curves, and only the slowly diffusing component remained, which points toward quasi-permanent entanglement of nanoparticles in the dense network. From the amplitudes of the two-components fit, the fraction of the fast and slowly diffusing G5-^{19}F dendrimers could be obtained (Supporting Information, Figure S1.1). The fractions of slowly diffusing G5-^{19}F nanoparticles as obtained by SE-PFG NMR decreased with the increasing Na^+ concentration from 0.15 at [Na^+] = 0 mM to 0.02 at [Na^+] = 200 mM, confirming the initial hypothesis that Na^+ ions reduce the phase volume of the dense network. Beyond this analysis, we did not quantify the phase volumes of the dense networks from the fraction of slowly diffusing nanoparticles, given their strong dependence on the particle concentration itself.

Network Heterogeneity Probed by FRAP and RICS. We repeated similar experiments as the PFG NMR studies using fluorescent G5-ATTO 488 nanoparticles, which are of the same design and size as G5-^{19}F. The presence of the ATTO 488 fluorophore enabled confocal laser scanning microscopy (CLSM) measurements that allow for the spatial localization of the trapped nanoparticles. In the gel samples loaded with fluorescent G5-ATTO 488 nanoparticles, the CLSM-based techniques FRAP and RICS complement each other with respect to the range of self-diffusion coefficients they can probe. By FRAP, after a bleaching pulse, the fluorescence is seen to recover, but only partly. Figure 5A shows a representative fluorescence recovery curve, indicating a very low diffusion coefficient for the slower fraction, which is difficult to quantify from FRAP because of background bleaching effects. To further shed light on this slow diffusing population, we used RICS to determine the diffusion coefficient of the slow fraction. RICS is an image correlation technique that works well for the determination of the diffusivity of diluted fluorescent particles by analysing their intensity fluctuations. For this reason, RICS measurements are

DOI: 10.1021/acs.langmuir.8b01052
Langmuir 2018, 34, 11110−11120

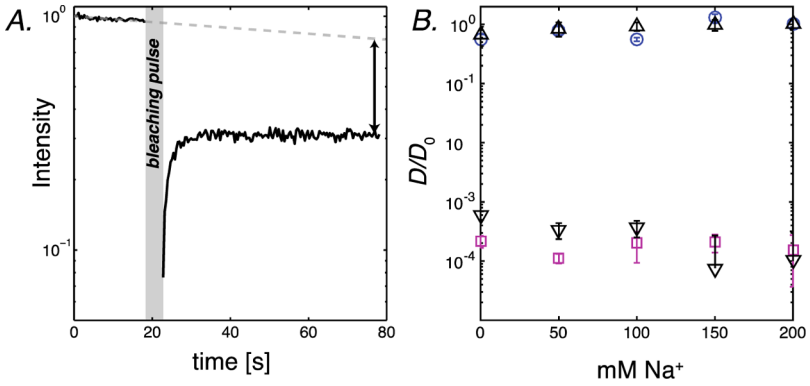

Figure 5. (A) Example of a FRAP curve (G5-ATTO 488 nanoparticle in a 2 wt % κ-carrageenan gel prepared with 20 mM K^+ and 0 mM Na^+) showing initial recovery of fluorescence after bleaching, after which the recovery levels off. The pre-bleach part of the curve shows gradual decay of fluorescence over the course of the measurement (bleaching during scanning), because of which, it is problematic to reliably determine a diffusion coefficient for the slow fraction. (B) Diffusion coefficients of G5-ATTO 488 (d = 6.9 nm) nanoparticles in 2 wt % κ-carrageenan gels. The fast diffusion coefficient is determined by FRAP (○) whereby only the first 10 post bleach images were analyzed—via this approach the slow fraction, and the influence of bleaching during scanning could be disregarded during data analysis. These data are compared to the fast component from the ^{1}H PFG NMR data from Figure 4A (△). The diffusion coefficient of the slow fraction is determined by RICS on washed gels (□). These data are compared to the slow component from the ^{1}H PFG NMR data from Figure 4A (▽).

performed on washed gels. The bright regions in the RICS image in Figure 6A,B contain the G5-ATTO 488 nanoparticle

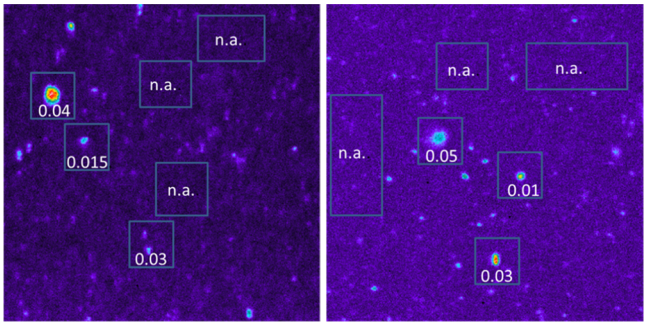

Figure 6. Localized estimation of diffusion coefficients of G5-ATTO 488 nanoparticles in κ-carrageenan gels prepared with 20 mM K^+ and 0 and 200 mM Na^+ via RICS. (left) 0 mM Na^+, $D_{avg} = 2 \times 10^{-14}$ m^2/s (averaged over the whole image). (right) 200 mM Na^+, $D_{avg} = 3 \times 10^{-14}$ m^2/s. Bright/red regions correspond to a stronger fluorescent signal, whereas dark/purple regions correspond to a weaker signal. The field of view is 24.7 μm.

probes, for which the self-diffusion coefficients of $D \approx 10^{-14}$ m^2/s (Figure 5B) were 3 orders of magnitude smaller than the ones determined by FRAP. This is in good agreement with the differences in diffusion constants found for the fast and the slowly diffusing component observed by PFG NMR (Figure 4A). Figure 5B shows the reduced diffusion coefficients for the fast and slow fractions obtained by FRAP and RICS, respectively. It can be seen that the self-diffusion coefficients of the fast and slow fractions differ by 3 orders of magnitudes, in agreement with the PFG NMR diffusometry results. Furthermore, the fraction of slowly diffusing G5-ATTO 488 probes decreases with the increasing Na^+ concentration in the gels, corroborating earlier findings by PFG NMR. The total fraction of slowly diffusing G5-ATTO 488 nanoparticles according to FRAP is higher than for the comparable G5-^{19}F nanoparticles according to PFG NMR (Supporting Information, Figure S1.1). This can be explained by the lower dose (0.05 wt %) of fluorescent G5-ATTO 488 nanoparticles used, as compared to G5-TEMPO, which will lead to a relatively high fraction of G5-ATTO 488 particles in the dense network, if the G5 particles are attracted to the dense network fraction of κ-carrageenan (as established in the discussion surrounding Figure 3B which showed that the nanoparticles first populate the dense network).

Heterogeneity of Water Self-Diffusion Probed by ODNP-Enhanced NMR Spectroscopy. In order to probe the solvent water self-diffusivity at the location of the G5 dendrimers, nanoparticles spin-labeled with paramagnetic TEMPO were employed. Figure 7 shows an example of a

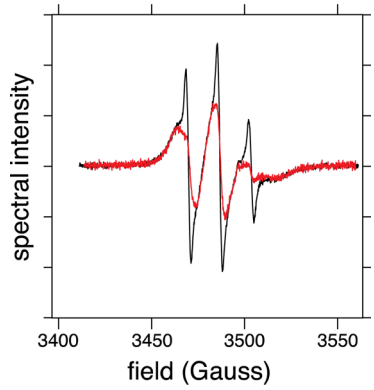

Figure 7. cw-EPR spectra of G5-TEMPO in 2 wt % κ-carrageenan gel induced with 0 mM Na^+/20 mM K^+ before (black line) and after (red line) the washing step.

cw-EPR spectrum of these G5-TEMPO nanoparticles in a 2% κ-carrageenan gel (in the presence of 20 mM K^+, 0 mM Na^+). Both a broad and a narrow component can be observed in the cw-EPR spectrum initially, but upon washing, the narrow features disappear from the spectrum. We assign the broad features of the remaining lineshape to particles immobilized in the dense network—this is corroborated by PFG NMR, FRAP, and RICS measurements that identified and described the immobilization of G5 nanoparticles in the dense network. From the difference between the double integral of both spectra, the fractions of immobilized G5-TEMPO particles can be estimated to be of the order 0.4−0.6 (Supporting

DOI: 10.1021/acs.langmuir.8b01052
Langmuir 2018, 34, 11110−11120

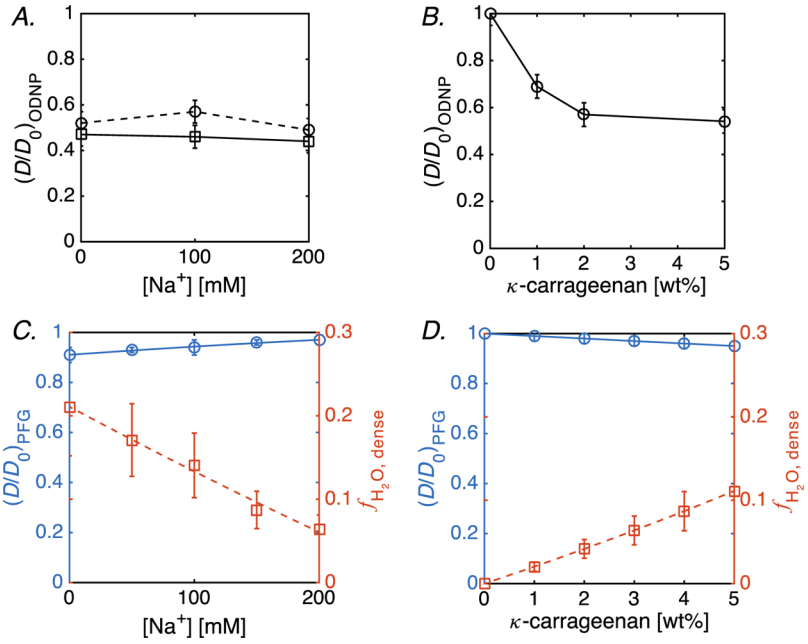

Figure 8. Retardation of local (reduced) water self-diffusion $(D/D_0)_{ODNP}$ as probed by G5-TEMPO in κ-carrageenan gels using ODNP-enhanced NMR spectroscopy in (A) 2 wt % κ-carrageenan gels induced with 0 mM Na^+, 20 mM K^+, before (○) and after (□) washing. The lines serve as guides the eyes. (B) κ-Carrageenan gels with weight fraction between 1 and 5 wt % induced at 200 mM Na^+/20 mM K^+. The solid line is a guide for the eyes. (C,D) Reduced self-diffusion coefficients of water $(D/D_0)_{PFG}$ as determined by PFG (blue circle, solid lines) and fraction of water in dense networks $f_{H_2O,dense}$ (red square, dashed lines) for (C) 2 wt % κ-carrageenan gels induced with 20 mM K^+ and 0−200 mM Na^+, (D) 0−5 wt % κ-carrageenan gels induced at 20 mM K^+, 100 mM Na^+. The solid and dashed lines are linear fits to the data.

Information, Figure S1.1). The fraction of immobilized G5-TEMPO particles as observed by EPR is higher than observed by PFG NMR (G5-^{19}F particles, d = 6.9 nm) and FRAP (G5-ATTO 488 particles, d = 6.9 nm), which may be attributed to their larger diameter (d = 11 nm). However again, given the apparent attraction to G5 nanoparticles to the dense network of κ-carrageenan, it is difficult to reliably extract the volume fraction of the dense network from the nanoparticle fraction. Critically, the presence of the TEMPO label allows for the probing of the short-range (nanometer scale) self-diffusivity of water within less than 1 nm of the spin labels attached to the G5 particles by the ODNP relaxometry effect,[16] as discussed next.

The dashed line in Figure 8A shows the ODNP-derived local water self-diffusion constants of water in the vicinity of the G5-TEMPO probes in 2% κ-carrageenan gels, induced with 0−200 mM Na^+ (fixed 20 mM K^+ concentration), over that of the same G5-TEMPO particles in solution. Of note, the local water diffusivities near G5-TEMPO in the κ-carrageenan gel was found to be $D = 1.3-1.4 \times 10^{-10}$ m^2/s compared to $D = 2.9 \times 10^{-10}$ m^2/s near G5-TEMPO in bulk aqueous solution. Compared to the self-diffusion constant of water 2.3×10^{-9} m^2/s, the latter value entails a retardation factor of ∼8, which is toward the higher end, but still within the range, of surface water diffusivity found on biomolecular surfaces by ODNP.[22,23] Whereas excluded volume effects are believed to only account for a reduction of a factor of 2, larger retardation factors can originate from the modulation of hydrogen bonding strength of water at hydrophilic surfaces, to date reported on protein, liposome, and silica nanoparticle surfaces.[24,29] Furthermore, in the G5-TEMPO nanoparticles, the paramagnetic moiety is positioned near the dendrimer surface; as a consequence, the reduced diffusivity of water in the PEG corona is also contributing to the basal diffusion retardation observed on the surface of these nanoparticles. However, of focus here is the *change* in the retarded surface water diffusivities near G5-TEMPO nanoparticles in the κ-carrageenan gel compared to in solution, with their ratio D/D_0 found to be 0.5. Because the effect of the G5 surface itself is already accounted for by taking the ratio of diffusion from the G5-TEMPO surfaces, this additional diffusion retardation of a factor of ∼2 reflects on the altered solvent diffusivity around the local environment of the nanoparticles. Interestingly, the observed reduced diffusivity around G5-TEMPO surfaces remains at $D/D_0 \approx 0.5$ irrespective of the Na^+ concentration, that is, with changes in the coarse mesh size, at 2% κ-carrageenan. Furthermore, the ODNP-derived local water self-diffusivity was measured again after a washing step that removes the mobile dendrimers. As indicated with a solid line in Figure 8A, no significant effect was observed on the apparent surface water diffusion coefficient around G5-TEMPO nanoparticles upon washing. This was unexpected because before the washing step, the apparent local water diffusivity was expected to be an average of the diffusivity around the mobile and immobile nanoparticles. Given that the washing step has been shown to remove the freely diffusing nanoparticles from the coarse pores of κ-carrageenan, we conclude that the ODNP effect around G5-TEMPO is dominated by the self-diffusion of water near dendrimers trapped within the dense network domains, and that the fraction or effect of the fast diffusing dendrimers in the coarse pores of κ-carrageenan is small (dashed vs solid lines in Figure 8A). This result shows that the diffusivity of water within the dense network of κ-carrageenan, in the vicinity of the polymer strands, is slowed by a factor of 2 compared to in the coarse pore volumes of the κ-carrageenan gel. This finding is the basis for the dark coloring given in the schematic representation of the dense network of κ-carrageenan in Figure 1 to illustrate

DOI: 10.1021/acs.langmuir.8b01052
Langmuir 2018, 34, 11110−11120

that the solvent diffusivity itself, and according to the Stokes−Einstein relation (even if valid approximately only for the local volume) the solvent viscosity, is altered in the dense network, not only the physical density of the strands. In other words, the hydrogen bond property of the water network is altered in the dense network of κ-carrageenan.

Next, local water diffusivities as probed by ODNP with G5-TEMPO particles are presented in Figure 8B in gels prepared with increasing (1−5%) κ-carrageenan levels. These gels were induced with 200 mM Na^+/20 mM K^+, which favors the formation of a coarse network. On this occasion, when the total concentration/density of the κ-carrageenan gel is varied, the reduced local water diffusion constants around G5-TEMPO remains robustly at D/D_0 = 0.5 at 2 and 5% κ-carrageenan levels irrespective of Na^+ concentrations but increases to D/D_0 = 0.7 at 1% κ-carrageenan levels. This result shows that decreasing the κ-carrageenan concentration below a threshold value leads to a significant loss in the dense network domains, leading to D/D_0 = 0.7 (i.e., smaller diffusion retardation).

The intricate relation between the fraction of slow diffusing nanoparticles and their concentration and size impedes straightforward estimation of the relative phase volume of the dense network. ODNP experiments performed with the G5-TEMPO particles yield a key unknown, namely, the relative (nanoscale) self-diffusion coefficient of water in the dense network, $(D/D_0)_{H_2O,dense}$, ≈0.5. We consider this value equivalent to the measured relative self-diffusion coefficient of water in the dense network. In contrast to ODNP, PFG NMR measures the water diffusivity averaged over the observation time, here Δ = 200 ms, spanning an rmsd of tens of micrometers. CLSM images showed that the size of the heterogeneities in κ-carrageenan gels are well below 10 μm. Hence, we can safely assume that the self-diffusion coefficients of water as probed by PFG NMR are averaged by diffusional exchange throughout these (sub-)micronscale heterogeneities. The averaged self-diffusion coefficients of water as measured by PFG NMR are presented in Figure 8C (dashed lines) for gels induced at different Na^+ concentrations (0−200 mM), and in Figure 8D for gels prepared with different κ-carrageenan concentrations (0−5 wt %). Small but distinct effects of the Na^+ concentration and κ-carrageenan concentrations on the reduced self-diffusion coefficient $(D/D_0)_{H_2O,PFG}$ can be observed (in solid line) with the expected trends. Given this, we can write $(D/D_0)_{H_2O,PFG}$ as a weighted average of $(D/D_0)_{H_2O,coarse}$ and $(D/D_0)_{H_2O,dense}$

$$\left(\frac{D}{D_0}\right)_{H_2O,PFG} = f_{H_2O,dense}\left(\frac{D}{D_0}\right)_{H_2O,dense} + (1 - f_{H_2O,dense})\left(\frac{D}{D_0}\right)_{H_2O,coarse} \quad (9)$$

Here, $f_{H_2O,dense}$ is the fraction of water in the dense network, which we assume to be proportional to the phase volume of the dense network (dark region in Figure 1). We estimate that $D_{H_2O,coarse}$ is equal to the bulk diffusion coefficient of water (D_0 = 2.7 × 10^{-9} m^2/s), while $(D/D_0)_{H_2O,dense}$ is set to be 0.5, informed by ODNP measurements using G5-TEMPO in washed κ-carrageenan gels. Taken together, we can calculate $f_{H_2O,dense}$ in a straightforward manner using the relationship shown in eq 9. The results of the so calculated $f_{H_2O,dense}$ fractions of κ-carrageenan gels prepared with different Na^+ concentrations (0−200 mM) and κ-carrageenan concentrations (0−5 wt %) are shown in Figure 8D. At a κ-carrageenan concentration of 2% and with an increasing Na^+ concentration from 0 to 200 mM, we observe a decrease of $f_{H_2O,dense}$ from approximately 0.2 to less than 0.1, that is, a reduction by 50% (Figure 8C), while at a Na^+ concentration of 200 mM and for κ-carrageenan concentrations between 0 and 5%, we observe $f_{H_2O,dense}$ to increase from 0 to approximately 0.1 (Figure 8D). We reiterate that the presence of a dense network was verified by means of CLSM with fluorescent G5-ATTO 488 nanoparticles. When these gels were washed, a fluorescence signal of trapped nanoparticles remained visible. Integration of the fluorescence level in these CLSM images showed an approximate 50% decrease in their concentration with the increasing Na^+ concentration (Supporting Information, S5), independently corroborating the just discussed trend for $f_{H_2O,dense}$ with the Na^+ concentration. We note that eq 9 also describes the averaging of the self-diffusion constants of G1-^{19}F and G3-^{19}F due to exchange between the dense and coarse domains (Figure S4.1,2). Because no independent estimate can be given for the self-diffusion constants of G1 and G3 in the dense domains, we have refrained from further modeling our experimental results for the G1-^{19}F and G3-^{19}F particles.

Interaction of a Low-Molecular Weight Solute with the κ-Carrageenan Network. We also assessed the interaction of the κ-carrageenan network with paramagnetic and nonparamagnetic analogues of low-molecular weight solutes. The ODNP-derived local water diffusivities for free paramagnetic 4-amino-2,2,6,6-tetramethylpiperidine-1-oxyl (4A-TEMPO) were measured and found to decrease with the κ-carrageenan concentration (Figure 9A, □), however, with smaller effect size compared to the retardation observed with G5-TEMPO particles (Figure 8A). Given the small size of 4A-TEMPO, we can expect rapid exchange between the coarse and dense networks, while ODNP will faithfully capture the weighted average diffusivity experienced by 4A-TEMPO. Given that ODNP-derived measurement of the local water diffusivity relies on the flip-flop rate between the electron and nuclear spins in the ps regime, 4A-TEMPO probes will capture the distinct diffusivities of water in these domains. Hence, the measured D/D_0 by ODNP, $(D/D_0)_{4A\text{-}TEMPO,ODNP}$ can be considered the weighted average between 4A-TEMPO in the dense versus coarse phase of the network

$$\left(\frac{D}{D_0}\right)_{4A\text{-}TEMPO,ODNP} = f_{dense,4A\text{-}TEMPO}\left(\frac{D}{D_0}\right)_{G5\text{-}TEMPO,dense} + (1 - f_{dense,4A\text{-}TEMPO})\left(\frac{D}{D_0}\right)_{coarse} \quad (10)$$

Here, $(D/D_0)_{G5\text{-}TEMPO,dense}$ is the local (reduced) water self-diffusion probed by G5-TEMPO in the dense network, as earlier determined to be 0.5, $(D/D_0)_{coarse}$ is equal to one, and $f_{dense,4A\text{-}TEMPO}$ is the fraction of 4A-TEMPO in the dense network. The fractions $f_{dense,4A\text{-}TEMPO}$ are presented in Figure 9B (□) and are approximately four times as larger as

DOI: 10.1021/acs.langmuir.8b01052
Langmuir 2018, 34, 11110−11120

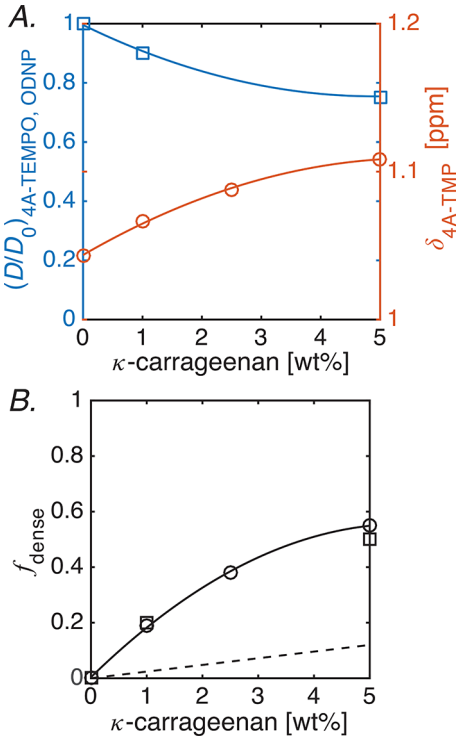

Figure 9. Effect of the κ-carrageenan concentration on (A) the chemical shift (δ) of (diamagnetic) 4A-TMP (right axis, red circle, data points are fitted with a two-site fast chemical exchange model) and local water self-diffusion $[(D/D_0)_{ODNP}]$ as probed by (paramagnetic) 4A-TEMPO using ODNP-enhanced NMR spectroscopy (left axis, blue square, solid curve serves as a guide for the eyes). (B) Population of TEMPO analogues present in the dense network (f_{dense}) as determined from local water self-diffusion (4A-TEMPO, □) and chemical shift perturbations (4A-TMP, ○). The solid line represents the binding curve obtained by fitting the chemical shifts perturbations of 4A-TMP by means of a two-site fast chemical exchange model. The dashed line indicates the phase volume of the dense network (Figure 8D).

previously observed for the phase solvent volume of the dense network of κ-carrageenan, $f_{H_2O,dense}$ (presented in Figure 8B, and also as a dashed line in Figure 9B). This suggests a weak affinity of 4A-TEMPO to the dense domains, which calls for confirmation by chemical shift experiments. For 4A-TEMPO, such experiments are however impeded because of paramagnetic line broadening by the free electron on the nitroxide moiety. The diamagnetic analogue of 4A-TEMPO, 4-amino-2,2,6,6-tetramethylpiperdine (4A-TMP), provided us with an experimental handle to observe chemical shift perturbations. We indeed observed that the ^{1}H NMR signals of 4A-TMP shifted with the increasing κ-carrageenan concentration (Figure 9A, red circle), in line with rapid exchange between the chemical environments experienced by this molecule in the coarse and dense networks. The fraction of 4A-TMP present in the dense network ($f_{dense,4A\text{-}TMP}$) can be obtained by modeling the chemical shift effect by a two-site fast chemical exchange model (Figure 9B, ○), yielding fraction $f_{dense,4A\text{-}TMP}$ with an estimated (monomer-based) association constant of $K_a \approx 10$ [M] for the weak binding of 4A-TMP to κ-carrageenan. The fractions derived from chemical shift perturbations ($f_{dense,4A\text{-}TEMPO}$, ○) are similar to those obtained for 4A-TEMPO by ODNP ($f_{dense,4A\text{-}TEMPO}$, □), and thus provide quantitative confirmation of the weak affinity of 4A-TEMPO for the dense domains.

The presence of significant volumes (10−20%) of dense networks with reduced solvent water diffusivity/viscosity and positive affinity of solutes have never been considered in modeling molecular and particle transport in κ-carrageenan gels.[1,6] This finding is relevant for understanding of transport of solutes with hydrodynamic radii in the nm range, such as proteins, but also for solutes of lower molecular weights. Most modeling approaches so far considered gels as homogeneous networks—our results indicate that microstructural heterogeneity in terms of network density and spatially varying local water diffusivity needs to be considered to acquire a complete understanding of transport through biological networks, and to predict or design properties for applications, such as sensorial actives in similar biopolymer network systems.

CONCLUSIONS

We demonstrated the presence of heterogeneity in the microstructure and solvent water diffusivity in Na^+/K^+-induced κ-carrageenan gels. At low Na^+ levels, these gels comprise both coarse and dense networks as observed by bimodal self-diffusion of dendritic nanoparticles (d = 6.9 nm). The addition of Na^+ led to a more homogeneous coarse network, and a decrease of bimodal diffusion. The self-diffusion of the fast moving nanoparticles could be fully described by obstruction by a coarse network of gel strands. At short time scales (up to hundreds of milliseconds), the slow moving nanoparticles were found to diffuse ~10^3 times slower than the faster nanoparticles. However, at longer time scales, these slower moving nanoparticles were found to be essentially immobilized, verified by significant washing and subsequent detection that identified these nanoparticle fraction to be trapped in the dense network. Furthermore, ODNP-amplified NMR relaxometry measurements showed that the water self-diffusion, and by extension the local solvent viscosity, near the trapped TEMPO-functionalized nanoparticles in the dense network is retarded by about a factor of 2. From the so determined local diffusivities of water in the dense network according to ODNP, and by utilizing the apparent water diffusivity measured by PFG NMR to be a weighted average of water in the dense and coarse phase of the κ-carrageenan network, the phase volumes of water in the dense network could be estimated to be between 0.1 and 0.2. These findings together are captured by the schematic in Figure 1 that shows heterogeneous structures of coarse and dense volumes in κ-carrageenan gels, with the latter making up a nonnegligible fraction and displaying reduced solvent water diffusivity, as illustrated with a darker coloration. The reduced local water self-diffusion observed by ODNP NMR measurement of freely dissolved TEMPO spin labels in κ-carrageenan could be explained by their weak affinity to the dense network. The significant volume of the dense networks with nm-scale mesh sizes and retarded solvent diffusivities bears relevance for understanding and modeling the transport and release of high- and low-molecular solutes from heterogeneous κ-carrageenan gels. We may conjecture from the conclusion of our studies that the loading and release of small solutes may be effectively achieved by tuning their affinity to the dense κ-carrageenan network regions rather than their physical size, while the physical size of solutes will play a role above a threshold dimension.

DOI: 10.1021/acs.langmuir.8b01052
Langmuir 2018, 34, 11110−11120

■ ASSOCIATED CONTENT

Supporting Information

The Supporting Information is available free of charge on the ACS Publications website at DOI: 10.1021/acs.langmuir.8b01052.

Fractions slowly diffusing nanoparticles in κ-carrageenan gels as assessed by NMR, FRAP, and EPR; synthesis and characterization of TEMPO- and ATTO 488-labeled dendrimers; exponential fitting of G5-dendrimer ^{1}H NMR attenuation curves: goodness of fit; ^{1}H NMR attenuation curves for G1 and G3 dendrimers in 2 wt % κ-carrageenan; and assessment of the relative amount of the dense network in gels with the increasing Na^+ concentration by CLSM (PDF)

■ AUTHOR INFORMATION

Corresponding Author

*E-mail: john.vanduynhoven@wur.nl.

ORCID

Daan W. de Kort: 0000-0002-8831-2011

Songi Han: 0000-0001-6489-6246

Notes

The authors declare the following competing financial interest(s): J.P.M.v.D. is employed by a company that markets food products.

■ ACKNOWLEDGMENTS

Lonneke Zuidgeest (Unilever R&D, Vlaardingen, Netherlands), Jinsuk Song, and Kuo-Ying Huang (University of California, Santa Barbara) are acknowledged for their contributions to this work. N.L. and E.S. acknowledge the financial support from SuMo Biomaterials (VINNOVA) and the Swedish Foundation for Strategic Research, SSF (Material structures seen through microscopy and statistics). This research received funding from the Netherlands Organization for Scientific Research (NWO) in the framework of the Technology Area COAST.

■ REFERENCES

(1) de Kort, D. W.; van Duynhoven, J. P. M.; Van As, H.; Mariette, F. Nanoparticle diffusometry for quantitative assessment of submicron structure in food biopolymer networks. *Trends Food Sci. Technol.* **2015**, *42*, 13−26.

(2) Saalwächter, K.; Seiffert, S. Dynamics-based assessment of nanoscopic polymer-network mesh structures and their defects. *Soft Matter* **2018**, *14*, 1976−1991.

(3) de Kort, D. W.; Rombouts, W. H.; Hoeben, F. J. M.; Janssen, H. M.; Van As, H.; van Duynhoven, J. P. M. Scaling Behavior of Dendritic Nanoparticle Mobility in Semidilute Polymer Solutions. *Macromolecules* **2015**, *48*, 7585−7591.

(4) Bourouina, N.; de Kort, D. W.; Hoeben, F. J. M.; Janssen, H. M.; Van As, H.; Hohlbein, J.; van Duynhoven, J. P. M.; Kleijn, J. M. Complex coacervate core micelles with Spectroscopic Labels for Diffusometric Probing of Biopolymer Networks. *Langmuir* **2015**, *31*, 12635−12643.

(5) Masaro, L.; Zhu, X. X. Physical models of diffusion for polymer solutions, gels and solids. *Prog. Polym. Sci.* **1999**, *24*, 731−775.

(6) Einhorn-Stoll, U.; Drusch, S. Methods for investigation of diffusion processes and biopolymer physics in food gels. *Curr. Opin. Food Sci.* **2015**, *3*, 118−124.

(7) Sandrin, D.; Wagner, D.; Sitta, C. E.; Thoma, R.; Felekyan, S.; Hermes, H. E.; Janiak, C.; de Sousa Amadeu, N.; Kühnemuth, R.; Löwen, H.; et al. Diffusion of macromolecules in a polymer hydrogel: from microscopic to macroscopic scales. *Phys. Chem. Chem. Phys.* **2016**, *18*, 12860−12876.

(8) Hermansson, A.-M. Rheological and microstructural evidence for transient states during gelation of kappa-carrageenan in the presence of potassium. *Carbohydr. Polym.* **1989**, *10*, 163−181.

(9) Viebke, C.; Piculell, L.; Nilsson, S. On the Mechanism of Gelation of Helix-Forming Biopolymers. *Macromolecules* **1994**, *27*, 4160−4166.

(10) Hermansson, A.-M.; Eriksson, E.; Jordansson, E. Effects of potassium, sodium and calcium on the microstructure and rheological behaviour of kappa-carrageenan gels. *Carbohydr. Polym.* **1991**, *16*, 297−320.

(11) de Kort, D. W.; van Duynhoven, J. P. M.; Hoeben, F. J. M.; Janssen, H. M.; Van As, H. NMR Nanoparticle Diffusometry in Hydrogels: Enhancing Sensitivity and Selectivity. *Anal. Chem.* **2014**, *86*, 9229−9235.

(12) Lorén, N.; Nydén, M.; Hermansson, A.-M. Determination of local diffusion properties in heterogeneous biomaterials. *Adv. Colloid Interface Sci.* **2009**, *150*, 5−15.

(13) Lorén, N.; Shtykova, L.; Kidman, S.; Jarvoll, P.; Nydén, M.; Hermansson, A.-M. Dendrimer Diffusion in κ-Carrageenan Gel Structures. *Biomacromolecules* **2009**, *10*, 275−284.

(14) de Kort, D. W.; Hoeben, F. J. M.; Janssen, H. M.; Bourouina, N.; Kleijn, J. M.; van Duynhoven, J. P. M.; Van As, H. 19F Labelled Polyion Micelles as Diffusional Nanoprobes. *Magnetic Resonance in Food Science; Defining Food by Magnetic Resonance*; Royal Society of Chemistry: Cambridge, 2015; pp 109−119.

(15) Armstrong, B. D.; Han, S. Overhauser Dynamic Nuclear Polarization To Study Local Water Dynamics. *J. Am. Chem. Soc.* **2009**, *131*, 4641−4647.

(16) Franck, J. M.; Pavlova, A.; Scott, J. A.; Han, S. Quantitative cw Overhauser effect dynamic nuclear polarization for the analysis of local water dynamics. *Prog. Nucl. Magn. Reson. Spectrosc.* **2013**, *74*, 33−56.

(17) Stejskal, E. O.; Tanner, J. E. Spin Diffusion Measurements: Spin Echoes in the Presence of a Time-Dependent Field Gradient. *J. Chem. Phys.* **1965**, *42*, 288−292.

(18) Johnson, E. M.; Berk, D. A.; Jain, R. K.; Deen, W. M. Hindered diffusion in agarose gels: test of effective medium model. *Biophys. J.* **1996**, *70*, 1017−1023.

(19) de Kort, D.; Van As, H.; van Duynhoven, J. Estimating microstructural length scales in κ-carrageenan hydrogels by PFG NMR nanoprobe diffusometry. *Proceedings of the XIII International Conference on the Applications of Magnetic Resonance in Food Science*; IM Publications, 2016; p 73.

(20) Jonasson, J. K.; Lorén, N.; Olofsson, P.; Nydén, M.; Rudemo, M. A pixel-based likelihood framework for analysis of fluorescence recovery after photobleaching data. *J. Microsc.* **2008**, *232*, 260−269.

(21) Digman, M. A.; Sengupta, P.; Wiseman, P. W.; Brown, C. M.; Horwitz, A. R.; Gratton, E. Fluctuation Correlation Spectroscopy with a Laser-Scanning Microscope: Exploiting the Hidden Time Structure. *Biophys. J.* **2005**, *88*, L33−L36.

(22) Ortony, J. H.; Cheng, C.-Y.; Franck, J. M.; Kausik, R.; Pavlova, A.; Hunt, J.; Han, S. Probing the hydration water diffusion of macromolecular surfaces and interfaces. *New J. Phys.* **2011**, *13*, 015006.

(23) Armstrong, B. D.; Han, S. A new model for Overhauser enhanced nuclear magnetic resonance using nitroxide radicals. *J. Chem. Phys.* **2007**, *127*, 104508.

(24) Barnes, R.; Sun, S.; Fichou, Y.; Dahlquist, F. W.; Heyden, M.; Han, S. Spatially Heterogeneous Surface Water Diffusivity around Structured Protein Surfaces at Equilibrium. *J. Am. Chem. Soc.* **2017**, *139*, 17890−17901.

(25) Hwang, L.-P.; Freed, J. H. Dynamic effects of pair correlation functions on spin relaxation by translational diffusion in liquids. *J. Chem. Phys.* **1975**, *63*, 4017−4110.

(26) Lee, C. H.; Crosby, A. J.; Emrick, T.; Hayward, R. C. Characterization of Heterogeneous Polyacrylamide Hydrogels by

DOI: 10.1021/acs.langmuir.8b01052
Langmuir 2018, 34, 11110−11120

Tracking of Single Quantum Dots. *Macromolecules* **2014**, *47*, 741−749.
(27) Hansing, J.; Netz, R. R. Particle Trapping mechanisms are different in spatially ordered and disordered interacting gels. *Biophys. J.* **2018**, *114*, 2653−2664.
(28) Reina, J. C.; Bansil, R.; Koňák, C. Dynamics of probe particles in polymer solutions and gels. *Polymer* **1990**, *31*, 1038−1044.
(29) Akdogan, Y.; Wei, W.; Huang, K.-Y.; Kageyama, Y.; Danner, E. W.; Miller, D. R.; Martinez Rodriguez, N. R.; Waite, J. H.; Han, S. Intrinsic Surface-Drying Properties of Bioadhesive Proteins. *Angew. Chem.* **2014**, *126*, 11435−11438.

DOI: 10.1021/acs.langmuir.8b01052
Langmuir 2018, 34, 11110−11120